PHILOSOPHICAL TRANSACTIONS OF THE ROYAL SOCIETY A

rsta.royalsocietypublishing.org

Research

Cite this article: Diemoz PC, Endrizzi M, Bravin A, Robinson IK, Olivo A. 2014 Sensitivity of edge illumination X-ray phase-contrast imaging. *Phil. Trans. R. Soc. A* **372**: 20130128. http://dx.doi.org/10.1098/rsta.2013.0128

One contribution of 16 to a Discussion Meeting Issue 'Taking X-ray phase contrast imaging into mainstream applications' and its satellite workshop 'Real and reciprocal space X-ray imaging'.

Subject Areas:
optics

Keywords:
X-ray imaging, phase-contrast imaging, signal-to-noise ratio, sensitivity

Author for correspondence:
P. C. Diemoz
e-mail: p.diemoz@ucl.ac.uk

Royal Society Publishing

Sensitivity of edge illumination X-ray phase-contrast imaging

P. C. Diemoz[1,2], M. Endrizzi[1], A. Bravin[3], I. K. Robinson[2,4] and A. Olivo[1,2]

[1]Department of Medical Physics and Bioengineering, University College London, London WC1E 6BT, UK
[2]Research Complex at Harwell, Harwell Oxford Campus, Didcot OX11 0FA, UK
[3]European Synchrotron Radiation Facility, Grenoble 38043, France
[4]London Centre for Nanotechnology, London WC1H 0AH, UK

Recently, we developed a theoretical model that can predict the signal-to-noise ratio for edge-like features in phase-contrast images. This model was then applied for the estimation of the sensitivity of three different X-ray phase-contrast techniques: propagation-based imaging, analyser-based imaging and grating interferometry. We show here how the same formalism can be used also in the case of the edge illumination (EI) technique, providing results that are consistent with those of a recently developed method for the estimation of noise in the retrieved refraction image. The new model is then applied to calculate, in the case of a given synchrotron radiation set-up, the optimum positions of the pre-sample aperture and detector edge to maximize the sensitivity. Finally, an example of the extremely high angular resolution achievable with the EI technique is presented.

1. Introduction

The possibility to achieve greatly improved image contrast, especially in the case of low absorbing materials, has motivated, in recent years, the development and application of numerous X-ray phase-contrast imaging (XPCi) techniques [1–8]. Besides the absorption

signal also encountered in conventional X-ray methods, the obtained images are characterized here by an additional 'phase-based' signal, which originates from the phase shift that X-rays experience upon passing through the imaged object. This phase shift is in turn proportional to the integral of the object's refractive index decrement over the X-ray path length [9].

The 'phase-based' signal observable in the images in most of the XPCi techniques has a differential nature, being to first approximation proportional to either the first spatial derivative of the phase shift [3,10] or to its second derivative [5]. As a result, while the absorption contrast is typically observed inside the sample structures, the phase contrast is stronger at their boundaries, where the largest variations in the refractive index arise.

The different form of this signal with respect to that provided by absorption dictates the need for a new definition of the signal-to-noise ratio (SNR), which is required in order to measure quantitatively the image quality and the visibility of the object details. On the one hand, this SNR can be used as a reference to optimize the acquisition parameters during the planning of an experiment and, on the other hand, it can be used to assess the image quality of acquired experimental images. Importantly, it also provides a common quantitative measure allowing the comparison of the signals provided by different XPCi techniques, for a given object and set-up parameters.

In recent publications [11,12], we have developed a theoretical framework for modelling the edge 'phase-based' SNR. This model was then applied for the theoretical and experimental estimation of the SNR for three different techniques: propagation-based imaging (PBI) [4,5], analyser-based imaging (ABI) [2,3] and grating interferometry (GI) [6,7].

In this article, we demonstrate how this theoretical model can be also applied to estimate the sensitivity of edge illumination (EI) XPCi, a technique currently under intensive development in the Radiation Physics Group at University College London (UCL) [13–18,20]. Besides, we show that the results are in agreement with the model developed in [20], in which the noise properties of retrieved maps of refraction angle were investigated. We then use the derived analytical expressions to study the dependency of the SNR upon the misalignment of the pre-sample and detector apertures, with reference to the set-up available at the ID17 beamline of the European Synchrotron Radiation Facility (ESRF, Grenoble, France), providing insights on possible strategies to optimize the image acquisition conditions. Finally, we show an example of an EI image acquired with the use of synchrotron radiation (SR), which demonstrates the very high sensitivity of the technique.

2. The edge signal-to-noise ratio for the propagation-based imaging, analyser-based imaging and grating interferometry techniques

Let us consider the simplified case of a non-absorbing object, and a parallel and monochromatic X-ray beam of wavelength λ (SR case). For a generic object edge, the SNR can be defined as [11]

$$\mathrm{SNR}_{\mathrm{edge,peak}} = \frac{A(I_{\max} - I_{\min})}{\sqrt{2A \cdot \mathrm{std}^2(I_{\mathrm{ref}}) + (\mathrm{noise}_{\mathrm{struct}})^2}}, \tag{2.1}$$

where A is the length of the edge (in units of the number of pixels along its longitudinal direction), and $I_{\min}$ and $I_{\max}$ are the minimum and maximum values of the pixel photon counts across the edge, respectively (averaged over A pixels). In the case where the edge profile features only one maximum (or minimum) peak, $I_{\min}$ (or $I_{\max}$) is replaced in equation (2.1) by the value of the intensity in a background region outside the edge, I_{ref}. 'std^2' is the square of the standard deviation, or variance of the referred quantity; $\mathrm{noise}_{\mathrm{struct}}$ indicates the contribution from the image structured noise.

The pixel noise can follow an essentially statistical or deterministic nature. The statistical noise is dependent on the number of photons detected by each detector pixel. As $I_{\max}$ and $I_{\min}$ can be assumed to be Poisson distributed, the uncertainty on their difference is equal to

$\sqrt{\mathrm{std}^2(I_{\max}) + \mathrm{std}^2(I_{\min})} \approx \mathrm{std}(I_{\mathrm{ref}})\sqrt{2} \approx \sqrt{2I_{\mathrm{ref}}}$. Note that we assume here the case of an ideal photon counting detector, where the number of counts is equal to the number of incident photons. The resulting equations, however, hold true also in the case of a non-ideal detector, if the statistical noise can be considered proportional to the square root of the number of counts (although in this case, a multiplication factor may need to be introduced, since $\mathrm{std}(I) \approx K\sqrt{I}$). Structured noise can have different origins: it can arise from detector response inhomogeneity, a spatially non-uniform beam and/or beam intensity fluctuating with time, inhomogeneities and/or instabilities in the optical components between the sample and the detector (e.g. the two gratings in GI, the analyser crystal in ABI and the detector edge in EI). The structured noise becomes prevalent when a high number of photons are considered, as the statistical noise becomes very small, while the latter is the dominant effect in the case of low photon statistics.

We will not review here the operational principles of the three considered XPCi techniques, the required set-ups and the expressions for the detected intensity, as they are thoroughly described in the literature. We just report, in the following, the analytical expressions for the edge SNR that can be derived from equation (2.1), under the assumption of pure statistical noise [11,12]:

$$\mathrm{SNR}_{\mathrm{PBI,peak}} = -\frac{\lambda d\sqrt{AI_0}}{2\pi\sqrt{2}}(\nabla^2_{\max}\phi_{\mathrm{conv}} - \nabla^2_{\min}\phi_{\mathrm{conv}}), \tag{2.2}$$

$$\mathrm{SNR}_{\mathrm{ABI,peak}} = \frac{\sqrt{AI_0}}{\sqrt{2}}\frac{R'(\theta_{\mathrm{an}})}{\sqrt{R(\theta_{\mathrm{an}})}}\Delta\theta_{y,\mathrm{conv}} \tag{2.3}$$

and

$$\mathrm{SNR}_{\mathrm{GI,peak}} = \frac{\sqrt{AT_{\mathrm{GR}}I_0}}{\sqrt{2}}\frac{G'(y_{\mathrm{G}};\Delta\theta_y = 0)}{\sqrt{G(y_{\mathrm{G}};\Delta\theta_y = 0)}}\Delta\theta_{y,\mathrm{conv}}, \tag{2.4}$$

where I_0 indicates the intensity incident on the object, d is the defocusing distance (PBI, equation (2.2)), R is the rocking curve and θ_{an} the angle of the analyser crystal (ABI, equation (2.3)), T_{GR} is the average transmission through the gratings, G the phase stepping curve and y_{G} the misalignment between the two gratings (GI, equation (2.4)). R' and G' indicate the first derivatives of R and G with respect to the refraction angle. $\phi_{\mathrm{conv}} = \phi * \mathrm{PSF}$ and $\Delta\theta_{y,\mathrm{conv}} = \Delta\theta_y * \mathrm{PSF}$, where ϕ is the object phase distribution, $\Delta\theta_y$ is the refraction angle in the direction of the system sensitivity (y) and PSF is the point-spread function of the imaging system.

The transport of intensity equation (corresponding to the geometrical optics approximation for PBI) has been used to derive equation (2.2) [5], the geometrical optics approximation and the linearization of the rocking curve R have been used in equation (2.3) [3], and the linearization of the phase-stepping function G has been used in equation (2.4) [10].

In §3, we show that the same approach presented above for the calculation of the edge SNR can be applied also in the case of the EI technique, and that an expression analogous to equations (2.2)–(2.4) can be obtained.

3. Calculation of the edge signal-to-noise ratio for the edge illumination technique

The EI technique is based on narrowing down the beam illuminating the object in one direction (y) with a slit, and analysing the radiation transmitted through it with the use of an absorbing edge in contact with the detector. The position of the edge, y_{edge}, is such that, when the object is absent, part of the beam falls on the edge and is thus stopped, while part is directly incident onto a line of detector pixels (figure 1). The edge can be used to chop either the lower or the upper part of the beam. However, as the two cases are perfectly symmetric, only the first condition is considered in the following.

If $S_{\mathrm{ref}}(y)$ indicates the beam distribution (number of photons per unit length in the y direction) incident on the edge when the object is absent, the number of photons recorded by an ideal

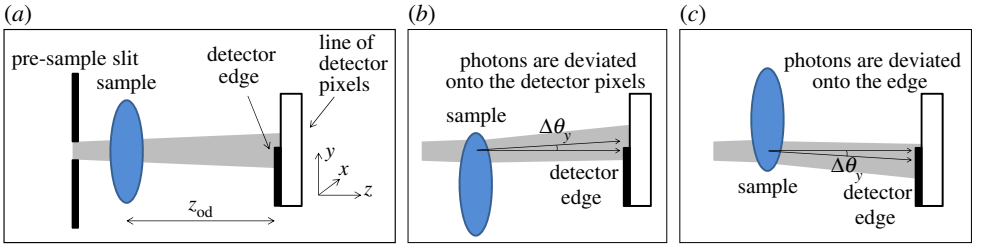

Figure 1. Diagram of the EI principle (not to scale). (Online version in colour.)

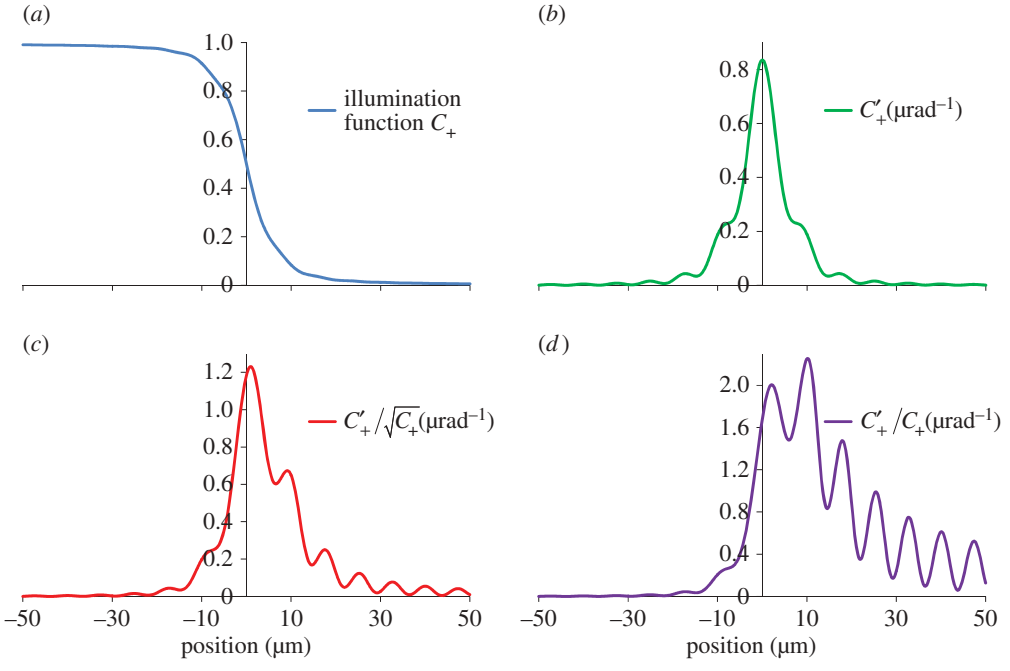

Figure 2. (*a*) Plot of the illumination curve C_+, as a function of the position of the detector edge, calculated numerically by means of Fresnel diffraction integrals [17]. (*b*) Plots of the first derivative of the illumination curve, C'_+, (*c*) of $C'_+/\sqrt{C_+}$ and (*d*) of C'_+/C_+. Experimental parameters considered in the calculation: source dimension = 24 μm, source-to-slit distance = 145 m, slit aperture = 20 μm, sample-to-detector distance = 10 m and X-ray energy = 85 keV. (Online version in colour.)

detector is equal to [19]

$$I_{\mathrm{ref},+}(y_{\mathrm{edge}}) = \int_{y_{\mathrm{edge}}}^{+\infty} \mathrm{d}y S_{\mathrm{ref}}(y) = I_0 C_+(y_{\mathrm{edge}}), \tag{3.1}$$

where $I_0 \equiv \int_{-\infty}^{+\infty} S_{\mathrm{ref}}(y)$ is the total beam intensity incident on the object and $C_+ \equiv \int_{y_{\mathrm{edge}}}^{+\infty} S_{\mathrm{ref}}(y)/I_0$ is the so-called illumination function, which is dependent on the position of the edge with respect to the beam and has values between 0 and 1 (figure 2*a*).

When the object is inserted in the beam at a distance z_{od} upstream of the detector edge, two effects usually take place: the overall beam intensity is reduced in amplitude owing to absorption inside the object, and the beam is shifted vertically by refraction (figure 1*b*,*c*). This leads to the following expression for the intensity incident on the detector, for a given position of the edge [19]:

$$I_{\mathrm{obj},+}(y_{\mathrm{edge}}) = TI_0 \cdot C_+(y_{\mathrm{edge}} - z_{\mathrm{od}} \cdot \Delta\theta_y), \tag{3.2}$$

where we have assumed the transmission T and the refraction angle $\Delta\theta_y$ to be constant within the size of the pre-sample slit. Let us now consider the case of negligible object absorption and small

refraction angles, the latter hypothesis being motivated by the fact that the aim of this analysis is to estimate the sensitivity of EI to weak object details. Under this assumption, the illumination function can be linearly approximated around y_{edge}:

$$I_{\mathrm{obj},+}(y_{\mathrm{edge}}) \simeq I_0 \cdot [C_+(y_{\mathrm{edge}}) + C'_+(y_{\mathrm{edge}})\Delta\theta_y], \tag{3.3}$$

where $C'_+(y_{\mathrm{edge}})$ is the first derivative of $C_+(y_{\mathrm{edge}})$ with respect to the refraction angle. Finally, by combining equation (3.3) with the definition of the edge SNR in equation (2.1), and by assuming pure statistical noise, the following expression is obtained:

$$\mathrm{SNR}_{\mathrm{EI,peak}} = \frac{\sqrt{AI_0}}{\sqrt{2}} \frac{C'_+(y_{\mathrm{edge}})}{\sqrt{C_+(y_{\mathrm{edge}})}} \Delta\theta_y = \frac{\sqrt{AI_0}}{\sqrt{2}} \frac{z_{\mathrm{od}} S_{\mathrm{ref},n}(y_{\mathrm{edge}})}{\sqrt{C_+(y_{\mathrm{edge}})}} \Delta\theta_y, \tag{3.4}$$

where $S_{\mathrm{ref},n} \equiv S_{\mathrm{ref}}/I_0$. Similarly to the ABI and GI techniques (equations (2.3) and (2.4), respectively), therefore, the SNR in EI is to first approximation proportional to the refraction angle. Likewise, it is also proportional to the function $C'_+/\sqrt{C_+}(y_{\mathrm{edge}})$: thus, C_+ plays the same role in determining the sensitivity as the functions R and G do for the ABI and GI techniques, respectively.

We now demonstrate that the expression here derived for the edge SNR in a single EI image is consistent with the results obtained in [19], where the noise in the retrieved refraction angle image was calculated. The refraction image can be obtained by mathematically combining two EI images of the same object, but acquired at complementary positions, with the edge chopping either the lower or the upper half of the beam [19]. The following analytical expression for the uncertainty on the refraction angle map was derived:

$$\sigma(\Delta\theta_y) \simeq \frac{1}{2z_{\mathrm{od}} S_{\mathrm{ref},n}(y_{\mathrm{edge}})\sqrt{TI_0}}. \tag{3.5}$$

Let us now assume that the object absorption is negligible ($T = 1$), and let us apply to the refraction angle image a definition for the edge SNR analogous to equation (2.1):

$$\mathrm{SNR}_{\mathrm{angle,peak}} = \frac{\sqrt{A}\Delta\theta_y}{\sqrt{2}\sigma(\Delta\theta_y)} \simeq \sqrt{2AI_0} z_{\mathrm{od}} S_{\mathrm{ref},n}(y_{\mathrm{edge}})\Delta\theta_y. \tag{3.6}$$

The expression for the refraction image SNR in equation (3.6) is very similar to the SNR for a single EI image given by equation (3.4). In particular, if we consider in the latter case a detector edge positioned at the centre of the beam, so that $C_+ = 0.5$, the only difference between the two formulae is a factor $\sqrt{2}$, i.e. $\mathrm{SNR}_{\mathrm{angle,peak}} = \sqrt{2} \cdot \mathrm{SNR}_{\mathrm{EI,peak}}$. This is explained by the fact that two images, instead of one, are used in the calculation of the refraction angle map, thus doubling the photon statistics and accordingly reducing the noise.

We now turn our attention to the analysis of the edge positions optimizing the SNR of a single EI image (see equation (3.4)). We consider, to this end, the set-up available at the ID17 beamline of the ESRF [18,19]. The vertical size of the virtual source is about 24 µm and the distance between the source and the pre-sample slit is 145 m; besides, we consider the following acquisition parameters (which partially match the experimental conditions used in [18,19]): pre-sample aperture = 20 µm, sample placed just downstream of the pre-sample slit, $z_{\mathrm{od}} = 10$ m and X-ray energy = 85 keV.

The illumination curve for this set-up and its first derivative with respect to the refraction angle have been calculated numerically with the use of Fresnel diffraction integrals [17], and are reported in figure 2*a*,*b*, respectively. We see that, S_{ref} being maximized at the centre of the beam, C'_+ is also maximum when the edge is at this position (figure 2*b*), which corresponds to an illuminated pixel fraction of 50% (i.e. $C_+ = 0.5$). However, the term $1/\sqrt{C_+}$ in equation (3.4) is large for low levels of illumination (figure 2*a*). Similarly to ABI and GI [11,12], therefore, there exists a trade-off between the two terms that maximizes the sensitivity. A plot of the quantity $C'_+/\sqrt{C_+}$ is reported in figure 2*c*, which shows that, in this particular set-up, a maximum for this function is obtained for a position of the edge very close to the centre of the beam. With reference

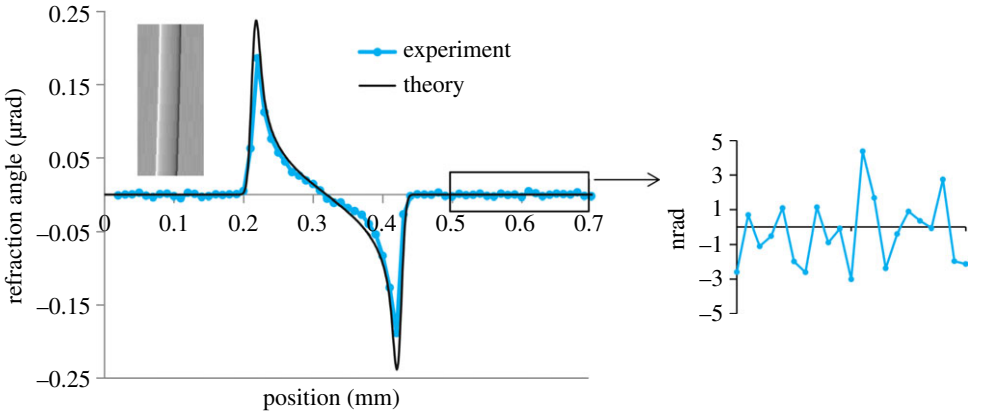

Figure 3. Retrieved refraction angle image of a 200 μm PEEK filament, obtained at the ESRF (ID17 beamline) at an energy of 85 keV. A profile across the filament and a zoomed view showing the noise level are shown. (Online version in colour.)

to equation (3.4), it can therefore be concluded that the edge SNR is maximized, for a fixed beam intensity I_0 incident on the object, at an illumination fraction slightly lower than 50%.

However, if the intensity on the detector is kept fixed rather than the intensity on the object, the edge SNR is maximized at a different position of the detector edge. In fact, noting that $I_{\mathrm{ref}} = C_+(y_{\mathrm{edge}})I_0$, equation (3.4) can be rewritten as

$$\mathrm{SNR}_{\mathrm{EI,peak}} = \frac{\sqrt{AI_{\mathrm{ref}}}}{\sqrt{2}} \frac{C'_+(y_{\mathrm{edge}})}{C_+(y_{\mathrm{edge}})} \Delta\theta_y. \tag{3.7}$$

A plot of the quantity C'_+/C_+ is presented in figure 2*d*. It shows that the maximum of this function is reached for a misalignment of about 10 μm from the centre of the beam, corresponding to a very low pixel illumination fraction, about 8%.

The radiation dose to the sample is proportional to the intensity incident on it. Therefore, if in a given experimental set-up the dose needs to be minimized (as is often the case for biological samples), the SNR optimization should be done by considering I_0 fixed, thus resulting in the maximization of $C'_+/\sqrt{C_+}$ (see equation (3.4)). If, instead, the bit depth of the detector represents the limiting factor of the acquisition and the dose is of less importance, the SNR should be optimized by keeping fixed the intensity I_{ref} on the detector and using equation (3.7) (thus resulting in a maximization of C'_+/C_+). These concepts had already been expressed in some previous publications on EI, where it was pointed out that low illumination levels could be used to achieve very high image contrast and sensitivity, although at the expense of the radiation dose to the sample [15,16]. However, they had not been yet understood at the mathematical level.

It is important to remark that, as the diffraction of the wave from the pre-sample slit is strongly dependent on the parameters used (e.g. the X-ray energy, the propagation distance, the pre-sample aperture, etc.), both the beam shape and the edge positions optimizing the SNR depend on the particular set-up under consideration. Therefore, the optimization of the edge position needs to be performed for every set of acquisition parameters, because it may provide considerably different results.

Finally, we present one example of the very high sensitivity achievable with the use of the EI technique in SR set-ups. It features a polyetheretherketone (PEEK) filament with a diameter of 200 μm, imaged at the ID17 beamline of the ESRF by using an energy of 85 keV. The vertical source size is 24 μm, the source-to-slit distance 145 m, the slit aperture 20 μm; the sample was placed 4.3 m downstream from the slit and the sample–detector distance was 6.0 m. In this case, two images of the object were acquired with the edge cutting the lower and the upper half of the beam, respectively, and were then combined to provide quantitative absorption and refraction maps. The exposure time for each of the two acquired images was 128 ms, which gave a number of

counts per detector pixel of about 30 000 (every count corresponding to an average of 48 recorded photons). The refraction image and a profile across the filament are presented in figure 3. Besides the good agreement achieved between the calculated angles and the theoretical ones, an extremely low level of noise is also obtained, below 2 nrad (as standard deviation in a background region). This means that angles of a few nanoradians are detectable by using this set-up, which is about one order of magnitude lower than values reported for other XPCi techniques directly sensitive to the first derivative of the phase (ABI and GI) [19–21], showing that EI enables the achievement of unprecedented angular resolution.

4. Conclusion

A theoretical model introduced in recent publications [11,12] for estimating the SNR of an edge phase-based signal has been extended here to the case of EI XPCi, a technique currently under intensive development at UCL. The analysis performed in this article shows that the signal in EI shares common features with the ABI and GI XPCi techniques. In particular, the SNR is directly proportional to both the first derivative of the phase shift and to a function of the illumination curve and its first derivative, $C'_+/\sqrt{C_+}$, which effectively defines the sensitivity of an EI set-up. It has been shown that the present model for the SNR in a single EI image is consistent with that used in [19], where the noise of the retrieved refraction image was estimated, analytically and through experiments.

The trend of the curve $C'_+/\sqrt{C_+}$ has been analysed as a function of the misalignment between the pre-sample and the detector apertures, and the results used to find the optimal working positions. For this purpose, the set-up available at the ID17 beamline of the ESRF was considered, as an example. However, the present formalism can be applied to any EI set-up. As the shape of the beam incident onto the detector is a complicated function of several experimental parameters, the optimal value for the aperture misalignment is expected to be different for various set-ups. In particular, the optimization of the sensitivity of laboratory-based set-ups using conventional sources is an interesting topic that will be the subject of forthcoming publications.

Through an example, we have also shown the extremely high sensitivity provided by the EI technique. The very high angular resolution is demonstrated by values for the noise in the refraction image below 2 nrad, representing an improvement of about one order of magnitude compared with values previously published for other XPCi techniques.

Acknowledgements. We acknowledge the European Synchrotron Radiation Facility for provision of beamtime through the in-house research programme and the personnel at the ID17 beamline for assistance in the experiment.

Funding statement. This work was supported by the UK Engineering and Physical Sciences Research Council (grant nos. EP/G004250/1, EP/I022562/1 and EP/I021884/1).

References

1. Bonse U, Hart M. 1965 An X-ray interferometer. *Appl. Phys. Lett.* **6**, 155–156. (doi:10.1063/1.1754212)
2. Davis T, Gao D, Gureyev TE, Stevenson AW, Wilkins SW. 1995 Phase-contrast imaging of weakly absorbing materials using hard X-rays. *Nature* **373**, 595–598. (doi:10.1038/373595a0)
3. Chapman D *et al*. 1997 Diffraction-enhanced X-ray imaging. *Phys. Med. Biol.* **42**, 2015–2025. (doi:10.1088/0031-9155/42/11/001)
4. Snigirev A, Snigireva I, Kohn V, Kuznetsov S, Schelokov I. 1995 On the possibilities of X-ray phase contrast microimaging by coherent high-energy synchrotron radiation. *Rev. Sci. Instrum.* **66**, 5486–5492. (doi:10.1063/1.1146073)
5. Gureyev TE, Nesterets YI, Stevenson AW, Miller PR, Pogany A, Wilkins SW. 2008 Some simple rules for contrast, signal-to-noise and resolution in in-line phase-contrast imaging. *Opt. Express* **16**, 3223–3241. (doi:10.1364/OE.16.003223)
6. David C, Nöhammer B, Solak H, Ziegler E. 2002 Differential X-ray phase contrast imaging using a shearing interferometer. *Appl. Phys. Lett.* **81**, 3287–3289. (doi:10.1063/1.1516611)

7. Momose A, Kawamoto S, Koyama I, Hamaishi Y, Takai K, Suzuki Y. 2003 Demonstration of X-ray Talbot interferometry. *Jpn. J. Appl. Phys.* **42**, L866–L868. (doi:10.1143/JJAP.42.L866)
8. Bravin A, Coan P, Suortti P. 2013 X-ray phase-contrast imaging: from pre-clinical applications towards clinics. *Phys. Med. Biol.* **58**, R1–R35. (doi:10.1088/0031-9155/58/1/R1)
9. Goodman JW. 2005 *Introduction to Fourier optics*, 3rd edn. Greenwood Village, CO: Roberts and Company Publishers.
10. Diemoz PC, Coan P, Zanette I, Bravin A, Lang S, Glaser C, Weitkamp T. 2011 A simplified approach for computed tomography with an X-ray grating interferometer. *Opt. Express* **19**, 1691–1698. (doi:10.1364/OE.19.001691)
11. Diemoz PC, Bravin A, Coan P. 2012 Theoretical comparison of three X-ray phase-contrast imaging techniques: propagation-based imaging, analyzer-based imaging and grating interferometry. *Opt. Express* **20**, 2789–2805. (doi:10.1364/OE.20.002789)
12. Diemoz PC, Bravin A, Langer M, Coan P. 2012 Analytical and experimental determination of signal-to-noise ratio and figure of merit in three phase-contrast imaging techniques. *Opt. Express* **20**, 27 670–27 690. (doi:10.1364/OE.20.027670)
13. Olivo A *et al*. 2001 An innovative digital imaging set-up allowing a low-dose approach to phase contrast applications in the medical field. *Med. Phys.* **28**, 1610–1619. (doi:10.1118/1.1388219)
14. Olivo A, Speller RD. 2007 A coded-aperture technique allowing X-ray phase contrast imaging with conventional sources. *Appl. Phys. Lett.* **91**, 074106. (doi:10.1063/1.2772193)
15. Olivo A, Speller RD. 2007 Modelling of a novel X-ray phase contrast imaging technique based on coded apertures. *Phys. Med. Biol.* **52**, 6555–6573. (doi:10.1088/0031-9155/52/22/001)
16. Olivo A, Speller RD. 2008 Image formation principles in coded-aperture based X-ray phase contrast imaging. *Phys. Med. Biol.* **53**, 6461–6474. (doi:10.1088/0031-9155/53/22/012)
17. Munro PRT, Ignatyev K, Speller RD, Olivo A. 2010 The relationship between wave and geometrical optics models of coded aperture type X-ray phase contrast imaging systems. *Opt. Express* **18**, 4103–4117. (doi:10.1364/OE.18.004103)
18. Olivo A, Diemoz PC, Bravin A. 2012 Amplification of the phase contrast signal at very high X-ray energies. *Opt. Lett.* **37**, 915–917. (doi:10.1364/OL.37.000915)
19. Diemoz PC, Endrizzi M, Zapata CE, Pešiæ ZD, Rau C, Bravin A, Robinson IK, Olivo A. 2013 X-ray phase-contrast imaging with nanoradian angular resolution. *Phys. Rev. Lett.* **110**, 138105. (doi:10.1103/PhysRevLett.110.138105)
20. Pfeiffer F, Bunk O, David C, Bech M, Ln G, Bravin A, Cloetens P. 2007 High-resolution brain tumor visualization using three-dimensional X-ray phase contrast tomography. *Phys. Med. Biol.* **52**, 6923–6930. (doi:10.1088/0031-9155/52/23/010)
21. Modregger P, Pinzer BR, Thüring T, Rutishauser S, David C, Stampanoni M. 2011 Sensitivity of X-ray grating interferometry. *Opt. Express* **19**, 18 324–18 338. (doi:10.1364/OE.19.018324)